Filter feeders and plankton increase particle encounter rates through flow regime control

Stuart Humphries[1]

Department of Animal and Plant Sciences, University of Sheffield, Western Bank, Sheffield S10 2TN, United Kingdom

Edited by David Karl, University of Hawaii, Honolulu, HI, and approved March 26, 2009 (received for review September 13, 2008)

Collisions between particles or between particles and other objects are fundamental to many processes that we take for granted. They drive the functioning of aquatic ecosystems, the onset of rain and snow precipitation, and the manufacture of pharmaceuticals, powders and crystals. Here, I show that the traditional assumption that viscosity dominates these situations leads to consistent and large-scale underestimation of encounter rates between particles and of deposition rates on surfaces. Numerical simulations reveal that the encounter rate is Reynolds number dependent and that encounter efficiencies are consistent with the sparse experimental data. This extension of aerosol theory has great implications for understanding of selection pressure on the physiology and ecology of organisms, for example filter feeders able to gather food at rates up to 5 times higher than expected. I provide evidence that filter feeders have been strongly selected to take advantage of this flow regime and show that both the predicted peak concentration and the steady-state concentrations of plankton during blooms are ≈33% of that predicted by the current models of particle encounter. Many ecological and industrial processes may be operating at substantially greater rates than currently assumed.

biological fluid dynamics | coagulation | phytoplankton | suspension feeding

Filter feeding animals are ubiquitous in aquatic habitats, with dense benthic assemblages exerting major effects on marine ecosystems through their impact on plankton populations (1). By removing particulate food from the surrounding water, filter feeders act as mediators of carbon flux between the water column and the bottom (1–3). Characterized by the possession of an organ used to capture suspended particles from the water, filter feeders use a highly variable array of feeding structures that include appendages bearing hairs, mucus or silk nets, gill rakers and baleen plates, lophophores, tentacles, and ciliated and flagellated cells. However, within a feeding structure, individual collecting elements (the first point of contact for food particles) are surprisingly similar in morphology because of the limited number of hydrodynamic mechanisms responsible for the delivery of particles (4–6). These encounter mechanisms are identical to those responsible for the majority of solid-fluid interactions in areas such as filtration, separation, chemical-, and bioreactors, and atmospheric particulate dynamics.

Currently, understanding of particle encounter mechanisms is limited to 2 simplified flow regimes: In low Reynolds number (Re) flows the effects of inertia are ignored, whereas in high Reynolds number flows effects of viscosity are neglected ($\mathrm{Re} = \rho U l/\mu$, where U is velocity, l is a linear dimension and ρ and μ are the density and dynamic viscosity, respectively, of the fluid). At low Re streamlines are symmetrical around a symmetrical object, whereas at high Re they are more closely packed and asymmetrical (Fig. 1). Thus, at some transitional Re, streamlines begin to compress around the body, providing a potential mechanism for increased encounter of particles following those streamlines (6). Although there continues to be considerable focus on interactions at high and low Re (variously "aerosol," "coagulation," or "flocculation" theory) we know much less about the transitional regime, characterized by Reynolds numbers in the range 0.1–50, where inertial and viscous forces are approximately balanced (refs. 4, 7, and 8, but see ref. 9 for an experimental study). In stark contrast to this bias in study, many particle processes involve Reynolds numbers in this range [for example: filter feeding animals (4, 6, 10–16, 17) ($\mathrm{Re} \geq 1$); marine snow formation (18) ($\mathrm{Re} = 0.4$–32); and for airborne pollen, spores and dust (19) ($\mathrm{Re} > 1$)].

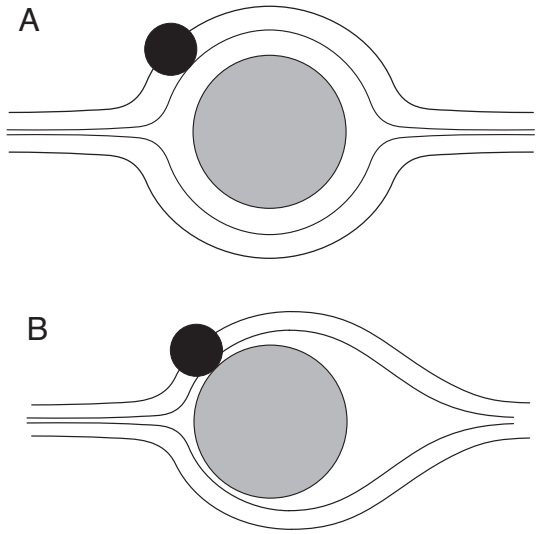

Fig. 1. Qualitative streamline patterns around a circular cylinder at low (*A*) and "intermediate" (*B*) Re values. Gray circle is cylinder in cross section. Note the compression of streamlines around the cylinder, and that the black circle (particle) following the same streamline in both cases will intercept the cylinder only in the intermediate Re case.

Here, I use a computational fluid dynamic (CFD) model to examine particle-fluid, particle-particle and particle-solid interactions in the range $0.1 \leq \mathrm{Re} \leq 50$ (hereafter "intermediate Re") where this transition occurs. Numerical approaches have proven invaluable in understanding more complex situations such as turbulent regimes, but are also useful for understanding the intermediate Re regime where analytical solutions become intractable. I show that, because of the compression of streamlines, encounter rates between particles, and between particles and structures, differ substantially from those predicted by low Re theory. I use the results to illustrate the importance of intermediate Re interactions to filter feeding animals and to flocculation driven by gravitational sedimentation (exemplified by coagulation of oceanic plankton).

Author contributions: S.H. designed research, performed research, analyzed data, and wrote the paper.

The authors declare no conflict of interest.

This article is a PNAS Direct Submission.

[1]To whom correspondence should be addressed at the present address: Department of Biological Sciences, University of Hull, Cottingham Road, Kingston-upon-Hull HU6 7RX, United Kingdom. E-mail: s.humphries@hull.ac.uk.

This article contains supporting information online at www.pnas.org/cgi/content/full/0809063106/DCSupplemental.

www.pnas.org/cgi/doi/10.1073/pnas.0809063106

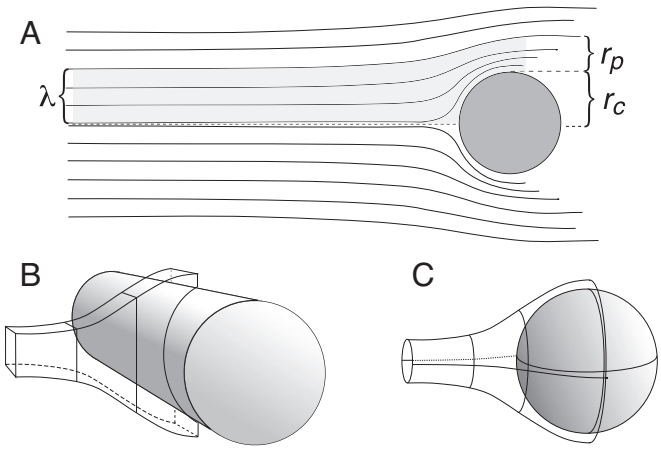

Fig. 2. Effectively swept region (λ) for a 2D collector (*A*), and the shape of the swept region for a cylinder (*B*) and a sphere (*C*).

Results

I constructed a finite element model for the simple case of an infinite cylindrical collector in an unbounded fluid (Fig. 2). This geometry represents a good approximation to both the food-collecting elements of animals such as polychaetes or cnidarians with widely spaced tentacles and of isolated filter fibres. The numerical simulations reveal that λ (half the cross-streamline distance of fluid whose particles are effectively encountered by the cylinder) is a function of both the Reynolds number based on the cylinder diameter (Re_c) and the absolute particle radius (r_p). This differs from the majority of low Re formulations, which are Re independent (5, 6). If restricted to $r_p \leq 0.5$ and $Re_c \leq 10$, λ estimated from the numerical simulations can be approximated to within 6.1% (0.1% for $Re_c \leq 0.1$) by

$$\lambda = \begin{cases} a_l + Re_c \cdot b_l & Re_c \leq 0.1 \\ a_i \cdot Re_c^{\,b_i} + c_i & 0.1 \leq Re_c \leq 10 \end{cases}, \qquad [1]$$

where

$$\begin{aligned} a_l &= 0.218 \cdot r_p^{1.938} \\ b_l &= 0.117 \cdot r_p^{1.923} \\ a_i &= 0.216 \cdot r_p^{1.954} \\ b_i &= 0.652 - 0.186 \cdot r_p \\ c_i &= 0.160 \cdot r_p^{1.911} \end{aligned}, \qquad [2]$$

Given λ, the rate of encounter between particles in the flow and the cylinder can be calculated as $F_R = 2CUl_c\lambda$, where C is the number concentration of particles in the fluid and l_c the length of the cylinder (Fig. 3). The dependency of encounter rate (F_R) on Re_c was derived from Eq. **1** for the intermediate Re regime:

$$F_R = \frac{2Cl_cRe^{1+b_i}\mu a_i}{r_c} + c_i \propto \begin{cases} Re_c^{1.652} & r_p \to 0 \\ Re_c^{1.559} & r_p = 0.5 \end{cases}. \qquad [3]$$

This indicates that, for an increasing Reynolds number, the particle encounter rate will increase faster than linearly with Re_c for $0.1 \leq Re_c \leq 10$. However, it will increase only proportionally to Re_c at $Re_c < 0.1$. At the smallest (0.005) and largest (0.5) r_p values considered, increasing Re_c from 0.1 to 1 increases encounter rate by a factor of ≈16, while from Re_c 1 to Re_c 10 increases F_R by a factor of 25.6 to 28.8 (Fig. 3). Compared with Re = 0.1, at Re = 10 F_R can be 470 times higher when the effects of increased particle delivery (increased U) and streamline compression (increased Re) are considered. The effect of streamline compression alone is an increase in F_R by a factor of

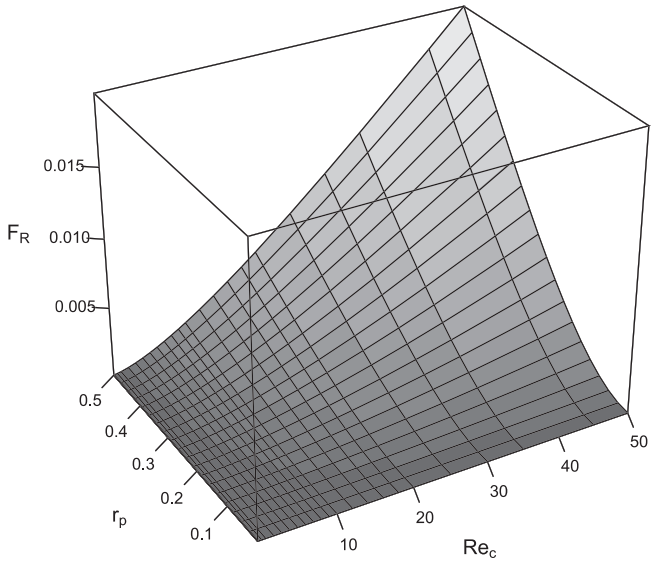

Fig. 3. Encounter rate (F_R) as a function of both collector Reynolds number (Re_c) and the particle radius (r_p). F_R calculations are based on unit particle concentration (C) and collector length (l_c). Note the rapid increase in encounter rate with $Re_c > 0.1$.

≈1.7 for an increase in Re from 0.1 to 1, ≈2.8 for Re 1 to 10, and ≈4.7 for Re 0.1 to 10.

Encounter rate F_R was converted to encounter efficiency (ε, see *Materials and Methods*), to allow comparison with semianalytical derivations (20) for $Re_c \ll 0.1$ and experimental data (9, see Fig. 4). The deviation from the low Re result of Fuchs (20) is more than likely due to his use of approximations to Lamb's flow (21). Despite these differences, the results support a consistent link between the high- and low-Re formulations of Fuchs (20), and the fit with the experimental data of Palmer et al. (9) for cylindrical collectors is

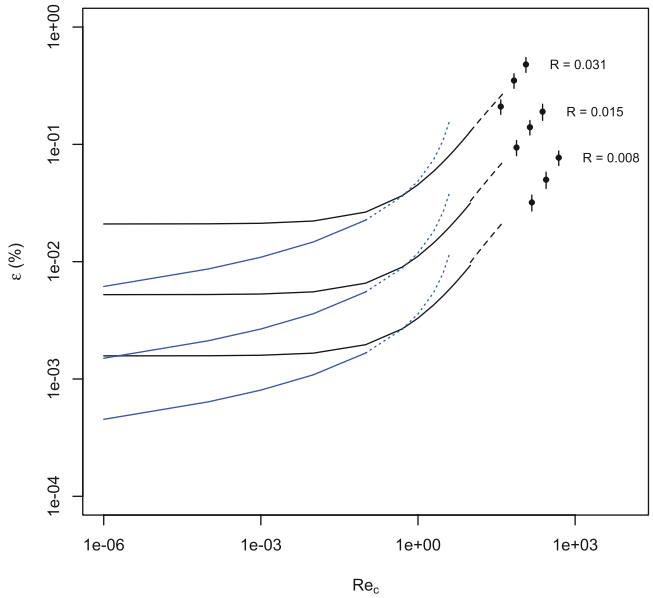

Fig. 4. Encounter efficiency (ε) as a function of collector Reynolds number (Re_c) for 3 values of r_p. Black lines are numerical results from this study (solid: $Re_c \leq 0.1$; broken: $0.1 \leq Re_c \leq 50$). Blue lines are the semianalytical derivations of ref. 20 (solid: $Re_c \leq 0.1$; dotted: extrapolated to $0.1 \leq Re_c \leq 4$). Note that the low-Re formulation predicts exponentially increasing encounter rates above its defined Reynolds number range ($Re \leq 0.1$). Points are means ± SE. of data from ref. 9.

ENGINEERING

ECOLOGY

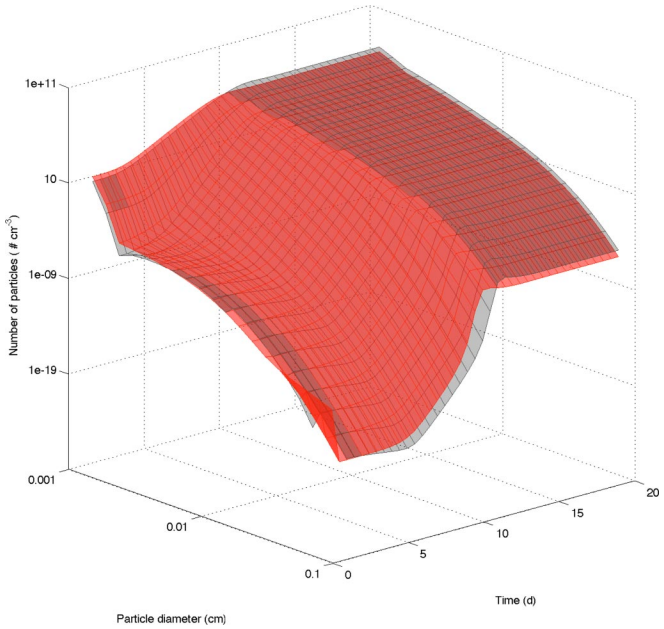

Fig. 5. 3D surface plots of particle number spectra from a model of algal floc formation by coagulation, using a curvilinear kernel (gray) and the intermediate Re kernel (red). Particle image diameter quantifies aggregate size; note the log scale on both *x* and *z* axes. Algal cell diameter = 10 μm, z = 20 m, η = 1 day^{-1}, α = 0.25, initial algal cell concentration = 0.1 cm^{-3}. Models do not include Brownian or shear coagulation kernels.

good, whereas the low-Re formulation predicts exponentially increasing efficiency for Re $>$ 0.1. This latter prediction is an extrapolation of Fuchs's formula outside its range of validity and is an artifact of the formulation.

A similar process to that of filter feeding is the collision of sinking spheres, which is one mechanism within coagulation theory (22). The aggregation of particles in the ocean, driven by collisions between particles, is an important process for the transfer of material from the upper layers of the ocean to the seabed, and is thought to be a mechanism by which plankton blooms terminate (23, 24). To examine the effects of intermediate Re on these processes I generated numerical results for encounter rates between 2 spheres (Fig. 2*C* and *Materials and Methods*). The resulting "coagulation kernels" describe the volume of fluid swept by a sphere, allowing the estimation of encounters between 2 spherical particles (25). Because the aim was to highlight the differences between low and intermediate Re effects for particle coagulation, 2 other kernels [Brownian and shear collision (22)] were not included, leaving only the effects of differential sedimentation (where particles collide because of differential sinking rates). The formulation of the intermediate Re kernel indicates that the relationship is proportional to the absolute cross-sectional area of the smaller particle. This relationship is similar to that for the commonly used curvilinear kernel, derived from the assumption of Stokes flow, whereas the less accurate rectilinear kernel is mostly dependent on the cross-sectional area of the larger particle.

Incorporation of the new kernel into a model of coagulation in a plankton bloom in the ocean surface layers (23, 26) provides evidence for the importance of including intermediate Re interactions in such systems. As expected (23), in both cases, as cells divide, the single-cell concentrations increase exponentially with time, whereas the concentration of aggregates decreases slowly as they settle out of the system (Fig. 5). As the concentration of single cells increases, coagulation becomes more important, resulting in a rapid increase in larger particles at around day 11 in the curvilinear case (Fig. 5). The intermediate Re case, however, experiences a much slower increase in single-cell concentrations, because collisions occur at a greater rate using the intermediate Re kernel (Fig. 5 and Fig. S1). Coagulation rates are higher in the intermediate Re case, leading to more rapid sedimentation of aggregates due to their increased sizes, resulting in a steady-state spectrum that is globally smaller (lower particle concentrations in each size class) than that predicted by the curvilinear kernel. Both the peak concentration of particles and the steady-state concentration are lower when the intermediate Re kernel is used. Peak particle numbers are highest for the single cells, and in this size class use of the intermediate Re kernel results in values 33.4% of that for the curvilinear case (3.2×10^7 vs. 9.5×10^7 cells per cubic centimeter), with the peak occurring 2 days earlier for the intermediate Re kernel (day 9 vs. day 11). The resultant steady-state spectrum is lower for the intermediate Re case (31.7% of curvilinear values: 2.7×10^7 vs. 8.5×10^7 cells per cubic centimeter) and, for the individual plankton cells, this state occurs a day earlier than for the curvilinear case (day 13 vs. day 14).

Discussion

The results presented here indicate the importance of considering a flow regime that falls between the main foci of most researchers. The implications of intermediate Re fluid dynamics for biology have been touched upon only rarely (6–9, 27, 28), and even less so for other disciplines. For instance, dramatic shifts in function have been attributed to movement of arrays of cylindrical structures at low to intermediate Re in lobsters and copepods (8). However, the effects of this regime on particle dynamics, and the mechanisms responsible have never been examined. In general it seems that particle dynamics in the intermediate Re regime offer filter feeding animals substantial gains in terms of encounters with food, and provide a mechanism to greatly enhance particle aggregation rates through sedimentation.

The results for cylindrical collectors should be considered from the perspective of the global importance of filter feeders in both ecological (1, 4) and economic (2, 29) contexts. To do so, using morphological measurements taken from the literature, I assessed the prevalence of intermediate Re regimes among filter feeders. Data were available for 113 filter feeding species ranging from single-celled protists to baleen whales (see Table S1). Feeding element diameter is bimodally distributed (Fig. 6*A*), indicating strong selection for 2 substantially different size ranges. This bimodality is potentially driven by the energetic benefits of operating in the intermediate Re regime, mediated by the inherent size-Re correlation in biological systems (large animals operate at higher Re). Thus, smaller filter feeders may be unable to reach "higher" Re, and indeed, those that use cilia and flagella may be limited to low Re because these organs are specifically adapted to produce movement in an environment where flows are reversible. Thirty-five (31%) of the species have collecting elements whose width is $>$90 μm wide (the modal size for the larger size peak), requiring a free stream velocity of just 11 mm·s^{-1} to result in Re_c = 1. Such velocities (however generated) are well within the range normally experienced by suspension-feeding organs (30–32). In comparison, at the modal size for the smaller peak (0.2 μm), a free stream velocity of 4.6×10^3 mm·s^{-1} is required for the same Re_c: Such high velocities are clearly unrealistic for small collectors. Suspension feeders are found in most extant animal taxa and several groups appear to span both size groups (Fig. 6*B*). Several of the animals positively identified in the literature as operating at intermediate Re have feeding elements substantially smaller than the modal 90 μm. Clearly, a large proportion of filter feeders are likely to be operating in the intermediate regime, thus reaping the benefits of the associated increase in food encounter rate. Nonetheless, most discussions of filter feeding dynamics implicitly assume that the low-Re formulations are valid (ref. 6; but see ref. 10 for an explicit example), and the lack of information on the

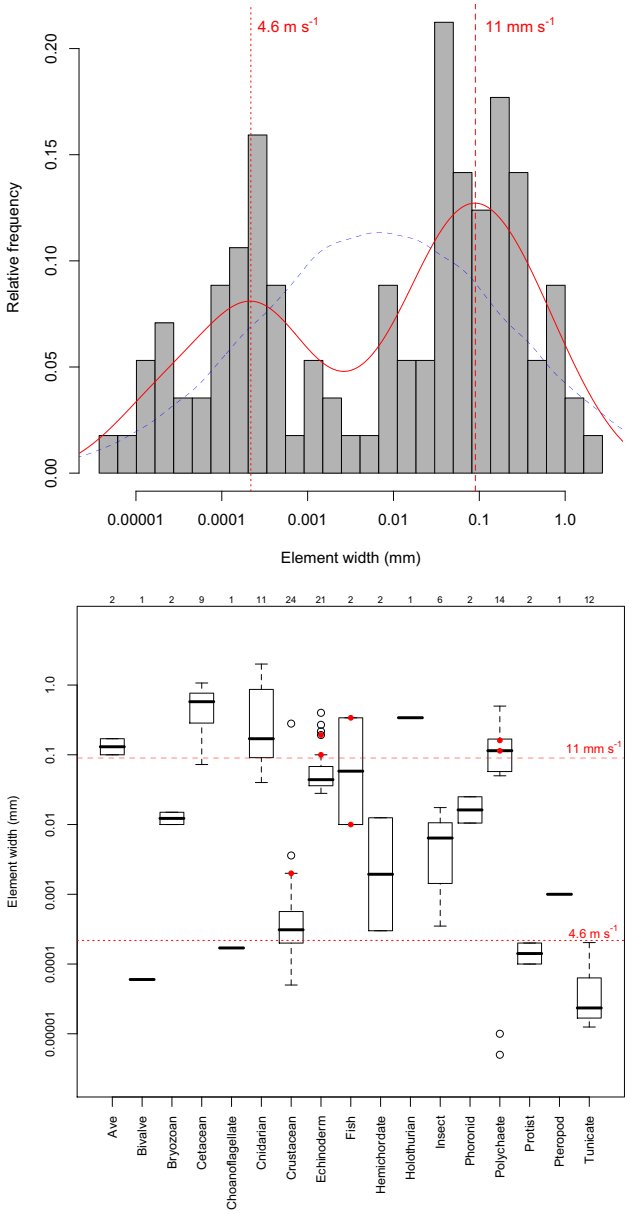

Fig. 6. Collecting element sizes in filter feeders. (*A*) Frequency histogram of log(collecting element width) for $n = 113$ filter feeders and corresponding density function (red line). Note the bimodal distribution of element sizes (for comparison, the dashed blue line gives the density function for a lognormal distribution with the same mean and variance as the data). Vertical red lines indicate the (free-stream) water velocity required to give $Re_c = 1$ at the bimodal peaks (note the difference in units between the two). (*B*) Box-and-whisker plot of element widths grouped within operational taxonomic units. Upper *x* axis gives the number of species in each group. Red horizontal lines are as vertical lines in main figure. Red dots are species reported to feed in the lab or field at $Re_c \geq 1$ (range 1 to 30) ((10–17);$n = 9$). All estimates assume $\mu/\rho = \nu = 1 \times 10^{-6}$.

intermediate Re regime means that the low-Re formulations are the only ones considered.

The model of coagulation within a plankton bloom shows that the formation of aggregates that operate in the intermediate Re regime leads to a cycle of increased encounter rates, increased aggregation rates and ultimately much more rapid removal of particulate carbon from the upper ocean than predicted by current models. Thus, intermediate Re interactions are likely to play a substantial part in oceanic particle dynamics, with follow-on implications for climate modeling and understanding of the global carbon cycle (33, 34).

Although the results here are generated using simplifying assumptions, a major concern in coagulation studies is the porosity of the aggregates formed by particle collisions (22, 35). Many marine aggregates have a fractal geometry and are therefore characterized using a fractal dimension (D) (with $D < 3$ indicating that the aggregate does not fill all of the available volume). Using a representative fractal dimension of 2.2 for the particles (36) in the plankton bloom model for both the intermediate Re and curvilinear kernels increases the rate of sinking of larger aggregates (as water is able to flow within the matrix of the aggregate), but has little qualitative effect on the bloom pattern, except that the intermediate Re case diverges further still from the pattern of the curvilinear kernel case. Interestingly, the kernel generated by the intermediate Re case (Fig. S1) falls between the rectilinear and curvilinear. This pattern, found in experimental studies has been explained by the fractal geometry of the aggregates (37), but given the Reynolds number involved (estimated at up to $Re = 1$) at least some of this effect may be due to intermediate Re dynamics.

The focus here on differential sedimentation is because of the clear relevance to streamline compression, but for field coagulation of phytoplankton, shear coagulation and differential sedimentation are often approximately equal in magnitude. The implications of intermediate Re for shear coagulation are not clear, but inclusion of current shear coagulation kernels in the model presented here would only qualitatively change the results as coagulation kernels are considered additive (22).

The assumption of point particles that do not perturb the flow field around the collector (see *Materials and Methods*) is the basis for the majority of plankton coagulation models, but clearly neglects a number of potentially important interactions. The most obvious is the potential for interaction of wakes between similarly sized particles. Incorporation of more accurate modeling of flow fields and surface interactions is possible (22, 38) and requires further study.

These results show that both predators and their planktonic or particulate prey can operate at intermediate Re, and that this flow regime has direct consequences for the ecology and evolution of aquatic ecosystems. Given the importance of filter feeders, plankton and suspended particles to both marine and fresh waters, the implications for understanding of aquatic food webs and nutrient cycling are great.

Although illustrated with biological systems, these results are directly relevant to reaction engineering and wastewater treatment; because identical methods are used to model reactions involving crystallization, flocculation and aerosol coagulation (39–42). Current research in these areas is based on low-Reynolds number kernels, valid for $Re \ll 1$ (based on the radius of the larger sphere). The intermediate Re kernel resulting from the numerical results differs substantially from those derived from low-Re number theory (Fig. S1). Given the fit of the numerical results to the solitary set of empirical data available (re.f 9 for the upper range of intermediate Re), the application of intermediate Re interactions to models of industrial processes could yield new improvements in reaction yield and filtration systems could be tuned to further optimise particle removal for industrial or medical uses.

In summary, these results expand current theory relating to the dynamics of particle-fluid systems, indicating increases in particle encounter rate at intermediate Re. To benefit from this flow regime the filtering organs of many extant filter feeders have been selected upon to operate in the intermediate Re regime. The importance of intermediate Re dynamics to a wide range of problems has hitherto been neglected, and these results suggest that the incorporation of such interactions across a large class of biological and physical problems should prove profitable in a diverse number of applications because many globally important fluxes (oceanic carbon cycling, precipitation), and applied applications (air filtration, industrial separation techniques) are driven by identical particle encounter processes.

Materials and Methods

Two finite element models were constructed and analyzed using the COMSOL Multiphysics package (COMSOL AB). Pathlines of massless particles following local velocity vectors were generated, and the results used to calculate the point of closest approach to the cylinder or sphere surface for particles released into the flow. The use of ''massless point particles'' that are essentially infinitely small and do not interact with the flow is routine in fluid dynamic studies, and as the flow field of the larger solid (i.e., the cylinder or the larger of 2 particles) tends to dominate the effect of the smaller particle in can be ignored (43, 44). The impact of the coagulation kernels on plankton floc formation was analyzed using a modified version of Jackson's (23) model of plankton growth coupled to aggregate formation. The basic model is freely available as Matlab code under the GNU public licence (26) at http://oceanz.tamu.edu/~ecomodel/Software/coagmodel/coagintro.html.

Model Construction. The computational domain for the cylinder (Fig. S2) consisted of a semicircle with a no-slip condition enforced on its circumference. The inlet condition on the left boundary was for steady flow, whereas the outlet on the right was for constant pressure. A symmetry boundary on the lower edge of the geometry reduced computational demands while a neutral boundary condition on the upper boundary simulated an infinite fluid domain (45). The spherical geometry was constructed in COMSOL's 2D axial symmetry mode, and differed from the cylindrical geometry only in that the symmetry boundary on the lower edge became a 2D axial symmetry boundary, also resulting in a slightly different mesh configuration (see below). The models were solved using a parametric solver to step up through Re_c values from 1×10^{-6} to 50, using the solution from previous step as the initial values for the next step. The parametric solver utilised a direct (UMFPACK) solver system.

To capture the flow characteristics close to the solid surface, the meshing interface in COMSOL was set to impose 2000 mesh elements on the solid boundary, resulting in a mesh with 34199 triangular elements, 167425 d.f. and a minimum element quality of 0.695 for the cylinder, and 35107 elements, 171511 d.f. and minimum element quality of 0.684 for the sphere. Mesh sensitivity was checked by varying the density of the mesh until the changes in the drag coefficient (C_D) of the cylinder section were $<1\%$, when the solution was assumed to be grid-independent. C_D was calculated by integrating the total stress (viscous + pressure) over the boundary of the cylinder to obtain the drag force (F_D), which could be inserted into:

$$C_D = 2\frac{F_D}{p \cdot U^2 \cdot 2 \cdot r_c}, \qquad [4]$$

where U is the free-stream velocity of the fluid, and r_c is the radius of the cylinder. Calculated values for C_D were compared with experimental and numerical results (46, 47) for drag on an infinite cylinder in steady flow at $Re_c \geq 6$, exhibiting good fit (Fig. S3). Qualitative analysis of the model shows the expected relaxation of streamline symmetry as Re_c increases as the magnitude of inertial effects approaches and then exceeds those of viscosity. During this transition, streamlines diverge and at $Re_c \approx 10$ separation of flow on the leeward face of the cylinder leads to the formation of a recirculation region anticipating the development of Von Karman vortices at still higher Re_c.

Effective Swept Region. Pathlines of massless point particles (following local velocity vectors) were generated in COMSOL, and the results used to calculate the point of closest approach to the cylinder surface for each of 60 particles distributed logarithmically along the left boundary from the point [0,0] on Fig. S2. The distance normal to the tangent of the cylinder surface to the point of closest approach for each particle gives the radius of the particle that will just intercept the cylinder (r_p), whereas the vertical distance from the point [0,0] to the particles release point gives the upstream region swept by the cylinder for particles of radius r_p. Dimensional analysis indicated that the effectively swept region (λ) was a function of both Re_c and the particle radius (r_p). Linear interpolation was used to provide a dataset to which functions of the form $\gamma = f(Re_c)$ were fitted. Regression splines were applied to the particle radius (r_p) and the coefficients of the γ functions to provide λ as a function of both Re_c and r_p. Here, the area swept by the cylinder is simply the effectively swept region from the 2D model, scaled by the projected frontal area of the cylinder (Fig. 2 *A* and *B*).

Encounter Efficiency. Encounter efficiency (ε) is defined as the rate of particle encounter of the cylinder (F_R), divided by the flux of particles approaching the cylinder (the number of particles that would pass through area occupied by the cylinder if it were not present). Thus, for the intermediate Re case we obtain

$$\epsilon = \frac{2CUl_c\lambda}{2CUr_c l_c} = \frac{\lambda}{r_c}, \qquad [5]$$

This can be compared with the semianalytical result of Fuchs (20) for $Re_c < 0.1$

$$\epsilon_{\text{Fuchs}} = \left((1+R) \cdot \ln(1+R) \frac{R \cdot (2+R)}{R \cdot (1+R)} \right) \Big/ (2.002 - \ln \text{Re}_c), \qquad [6]$$

where R is the ratio of particle and cylinder radii (r_p/r_c), as seen in Fig. 4.

Spherical collectors. The effectively swept region (λ) for the sphere (Fig. 2*C*) was obtained in the same way as for the cylinder. As for the cylindrical case, when restricted to $r_p \leq 0.5$ and $Re_s \leq 10$, λ_{sphere} can be approximated to within 2.5% (0.02% for $Re_s \leq 0.1$). However, in the case of the sphere the accuracy is still within 4% up to $Re_s = 40$ using:

$$\lambda_{sphere} = \begin{cases} a_l + Re_s \cdot b_l & Re_s \leq 0.1 \\ a_i \cdot Re_s^{b_i} + c_i & 0.1 \leq Re_s \leq 40, \end{cases} \qquad [7]$$

where

$$a_l = e^{0.141} \cdot r_p^{0.988}$$
$$b_l = e^{-2.370} \cdot r_p^{0.968}$$
$$a_i = e^{-1.637} \cdot r_p^{1.041}$$
$$b_i = 0.632 - 0.116 \cdot e^{r_p \times 1.424}$$
$$c_i = 0.160 \cdot r_p^{1.911}$$

These values were then used to calculate the ''differential sedimentation kernel'' (β) used in coagulation models:

$$\beta_{\text{int}} = \pi\lambda^2 |U_i - U_j|, \qquad [8]$$

where U_i and U_j are the velocities of 2 spheres settling due to gravity, and where Re used in the calculation of λ is based on the greater of the two U values. The differential sedimentation kernel describes the situation where one particle sinks faster than another and so catches up with it, leading to an interaction between the two. The use of the higher of the 2 particle velocities in the λ calculation follows from the assumption that the smaller, captured, particle has no effect on the flow field.

The intermediate collision kernel can be compared with those commonly used in coagulation theory, rectilinear (β_{rec}) and curvilinear (β_{cur}) kernels. The former describes particle-particle interactions with no hydrodynamic effect of the falling particles (effective swept area = projected frontal area):

$$\beta_{\text{rec}} = \pi(r_i + r_j)^2 |U_i - U_j|. \qquad [9]$$

whereas the curvilinear kernel incorporates the effect of flow at low Re around the larger of the 2 particles (effective swept area $\ll$ projected frontal area):

$$\beta_{\text{cur}} = 0.5\pi r_j^2 |U_i - U_j|, \quad \text{where } r_i \gg r_j. \qquad [10]$$

Algal Floc Model. A modified version of Jackson's (23) model of plankton growth coupled to aggregate formation was used to implement the intermediate Re kernel (Eq. **8**). The basic model is freely available as Matlab code under the GNU public licence (26) (http://oceanz.tamu.edu/~ecomodel/Software/coagmodel/coagintro.html). The model uses the sectional method (39, 40, 48) to transform the underlying Smoluchowski-type integro-differential equation into a series of coupled ordinary differential equations.

$$\frac{dn(m)}{dt} = \frac{\alpha}{2} \int_0^m \beta(m_j, m - m_j) n(m - m_j) dm_j - \alpha n(m) \int_0^\infty \beta(m, m_j) n(m_j) dm_j \qquad [11]$$

where the particle size spectrum $n(m)$ is given in terms of mass. The equation gives the rate of change in a continuous particle size spectrum due to the

addition or removal of particles from size classes (sections) due to collision (β) and subsequent sticking (α) of particles. The initial conditions assume equal particle mass in each section, which is then solved to find a steady-state spectrum to use as the starting point for the discretised coagulation equations. Coagulation is thus initiated by the presence of aggregates in the initial size spectrum.

The model considers an initial population of individual algal cells growing at a rate η by division into 2 daughter cells identical to the parent. Cells sink at a rate determined by their effective weight (based on density) and size, following Stokesian dynamics, as do aggregates that are formed when cells collide. Collisions are determined by the local cell concentration and by the interactions described by the collision kernel β. Cells and aggregates sinking from the simulation domain are removed from the population.

The code was further modified to correctly model sinking rates of particles or aggregations large or fast enough not to meet the assumptions of Stokes's law. Sinking rate was estimated by using the empirically-derived formulation of Brown and Lawler (49), which spans both the Stokes regime and Re up to $\approx$5000.

Model parameters were set to those used in Jackson (23), except in the implementation of the coagulation kernels (Table 1). Because the aim was to highlight the differences between low and intermediate Re effects for general particle coagulation systems, both Brownian and shear collision kernels were excluded from the model runs, leaving only the effects of differential sedimentation. Because of the limits of the approximations used for λ Eq. **8** the kernel β_{int} used a maximum Re of 40, above which the assumption Re = 40 was made for all interactions.

Table 1. Parameter values for the algal floc model

Parameter	
Algal cell diameter, μm	10
Algal growth rate (η), d^{-1}	1
Algal cell stickiness (α)	0.25
Algal cell excess density ($\Delta\rho$), $g{\cdot}cm^{-1}$	0.06428
Aggregate fractal dimension	3
Mixed-layer thickness (z), m	20
No. of sections*	25
Growth in aggregates until section	4
Average shear rate	Not implemented

*Within particle size spectrum (see *Materials and Methods*)

ACKNOWLEDGMENTS. I thank Graeme Ruxton, William Zimmerman, Mike Boots, and Lesley Morrell for providing insightful comments and support and 3 anonymous reviewers for providing constructive input that greatly improved the manuscript. This work was supported by Natural Environment Research Council Advanced Research Fellowship NE/B500690/1 (to S.H.). Engineering and Physical Sciences Research Council Grant EP/E01867X/1 (Bridging the Gap between Mathematics, Information and Communication Technology, and Engineering Research at Sheffield) provided funding for a minidiscipline hop that supported the computational modeling work.

1. Gili JM, Coma R (1998) Benthic suspension feeders: Their paramount role in littoral marine food webs. *Trends Ecol Evol* 13(8):316–321.
2. Wildish D, Kristmanson D (1997) *Benthic Suspension Feeders and Flow* (Cambridge Univ Press, Cambridge).
3. Wotton RS (1994) In *The Biology of Particles in Aquatic Systems*, ed Wotton RS (CRC, Boca Raton, FL), pp 181–204.
4. Humphries S (2007) In *Body Size: The Structure and Function of Aquatic Ecosystems*, eds Hildrew AG, Raffaelli DG, Edmonds-Brown R (CUP, Cambridge), pp 16–32.
5. Rubenstein DI, Koehl MAR (1977) The mechanisms of filter feeding: Some theoretical considerations. *Am Nat* 111:981–994.
6. Shimeta J, Jumars PA (1991) Physical mechanisms and rates of particle capture by suspension feeders. *Oceanog Mar Biol Ann Rev* 29:191–257.
7. Jiang HS, Meneveau C, Osborn TR (2002) The flow field around a freely swimming copepod in steady motion. Part II: Numerical simulation. *J Plankton Res* 24:191–213.
8. Koehl MAR (2000) Consequences of size change during ontogeny and evolution. *Scaling in biology*, eds Brown JH, West GB (Oxford Univ Press, Oxford), pp 67–86.
9. Palmer M, Nepf H, Petterson T, Ackerman J (2004) Observations of particle capture on a cylindrical collector: Implications for particle accumulation and removal in aquatic systems. *Limnol Oceanogr* 49:76–84.
10. Loo LO, Jonsson PR, Skold M, Karlsson I (1996) Passive suspension feeding in *Amphiura filiformis* (Echinodermata: Ophiuroidea): Feeding behaviour in flume flow and potential feeding rate of field populations. *Mar Ecol Prog Ser* 139:143–155.
11. Sanderson SL, Cech JJ, Cheer AY (1994) Paddlefish buccal flow velocity during ram suspension-feeding and ram ventilation. *J Exp Biol* 186:145–156.
12. Friedland KD (1985) Functional morphology of the branchial basket structures associated with feeding in the atlantic menhaden, Brevoortia tyrannus (Pisces: Clupeidae). *Copeia* 1985(4):1018–1027.
13. Shimeta J, Koehl MAR (1997) Mechanisms of particle selection by tentaculate suspension feeders during encounter, retention, and handling. *J Exp Mar Biol Ecol* 209:47–73.
14. Johnson A (1993) Sag-mediated modulated tension in Terebellid tentacles exposed to flow. *Biol Bull* 185:10–19.
15. Allen JR (1998) Suspension feeding in the brittle-star *Ophiothrix fragilis*: Efficiency of particle retention and implications for the use of encounter-rate models. *Mar Biol* 132:383–390.
16. Cheer AY, Koehl MAR (1987) Paddles and rakes: Fluid flow through bristled appendages of small organisms. *J Theor Biol* 129 17–39.
17. Koehl MAR (1995) Fluid flow through hair-bearing appendages: Feeding, smelling and swimming at low and intermediate Reynolds numbers. *Soc Exp Biol Symp*157–182.
18. Alldredge A, Gotschalk C (1988) In situ settling behavior of marine snow. *Limnol Oceanogr* 33:339–351.
19. Maus R, Umhauer H (1997) Collection efficiencies of coarse and fine dust filter media for airborne biological particles. *J Aerosol Sci* 28:401–415.
20. Fuchs NA (1964) *The Mechanics of Aerosols* (Pergamon, Oxford).
21. Lee KW, Liu BYH (1982) Theoretical-study of aerosol filtration by fibrous filters. *Aerosol Sci Tech* 1:147–161.
22. Burd AB, Jackson GA (2009) Particle Aggregation. *Ann Rev Mar Sci* 1(1):65–90.
23. Jackson GA (1990) A model of the formation of marine algal flocs by physical coagulation processes. *Deep Sea Res* 37:1197–1211.
24. Kiørboe T, Lundsgaard C, Olesen M, Hansen JLS (1994) Aggregation and sedimentation processes during a spring phytoplankton bloom—a field experiment to test coagulation theory. *J Mar Res* 52(2):297–323.
25. Jackson GA (2005) In *Flocculation in Natural and Engineered Environmental Systems*, eds Droppo I, Leppard G, Liss S, Milligan T (CRC, Boca Raton), pp 271–292.
26. Jackson GA (2001) A simple coagulation model (Texas A&M University).
27. Jiang HS, Meneveau C, Osborn TR (1999) Numerical study of the feeding current around a copepod. *J Plankton Res* 21:1391–1421.
28. Ayaz F, Pedley TJ (1999) Flow through and particle interception by an infinite array of closely-spaced circular cylinders. *Euro J Mech B Fluids* 18:173–196.
29. Dame RF, Olenin S (2005) *The Comparative Roles of Suspension-Feeders in Ecosystems* (Springer, Berlin).
30. Leichter J, Witman J (1997) Water flow over subtidal rock walls: Relation to distributions and growth rates of sessile suspension feeders in the Gulf of Maine. *J Exp Mar Biol Ecol* 209:293–307.
31. Lesser M, Witman J, Sebens K (1994) Effects of flow and seston availability on scope for growth of benthic suspension-feeding invertebrates in the Gulf of Maine. *Biol Bull* 187:319–335.
32. Sebens K, Helmuth BST, Carrington E, Agius B (2003) Effects of water flow on growth and energetics of the scleractinian coral Agaricia tenuifolia in Belize. *Coral Reefs* 22:35–47.
33. De La Rocha CL, Passow U (2007) Factors influencing the sinking of POC and the efficiency of the biological carbon pump. *Deep Sea Res II* 54:639–658.
34. Raven J, Falkowski P (1999) Oceanic sinks for atmospheric CO 2. *Plant Cell Env* 22:741–755.
35. Burd AB, Jackson GA (2002) Modeling steady-state particle size spectra. *Environ Sci Technol* 36:323–327.
36. Jackson GA, Logan BE, Alldredge AL, Dam HG (1995) Combining particle-size spectra from a mesocosm experiment measured using photographic and aperture impedance (coulter and elzone) techniques. *Deep Sea Res II* 42:139–157.
37. Li XY, Logan BE (1997) Collision frequencies of fractal aggregates with small particles by differential sedimentation. in *Environ Sci Technol* 31(4):1229–1236.
38. Han M, Lawler DF (1991) Interactions of two settling spheres: Settling rates and collision efficiency. *J Hydraul Engineer* 117:1269–1289.
39. Debry E, Sportisse B (2007) Solving aerosol coagulation with size-binning methods. *Appl Numer Math* 57:1008–1020.
40. Hounslow M, Ryall RL, Marshall VR (1988) A discretized population balance for nucleation, growth, and aggregation. *AIChE J* 34:1821–1832.
41. Thomas D, Judd S, Fawcett N (1999) Flocculation modelling: A review. *Water Res* 33:1579–1592.
42. Grammatika M, Zimmerman WB (2001) Microhydrodynamics of flotation processes in the sea surface layer. *Dyn Atmos Oceans* 34:327–348.
43. Brown RC (1993) *Air Filtration: An Integrated Approach to the Theory and Applications of Fibrous Filters* (Pergamon, Oxford, UK).
44. Jackson GA (2001) Effect of coagulation on a model planktonic food web. *Deep-Sea Res I* 48:95–123.
45. Chang MW, Finlayson BA (1980) On the proper boundary-conditions for the thermal entry problem. *Int J Numer Meth Eng* 15:935–942.
46. Braza M, Chassaing P, Minh HH (1986) Numerical study and physical analysis of the pressure and velocity fields in the near wake of a circular cylinder. *J Fluid Mech* 165:79–130.
47. Takami H, Keller H (1969) Steady two-dimensional viscous flow of an incompressible fluid past a circular cylinder. *Phys Fluids* 12 (Suppl II):51–56.
48. Gelbard F, Tambour Y, Seinfeld J (1980) Sectional representations for simulating aerosol dynamics. *J Coll Interf Sci* 76:541–556.
49. Brown PP, Lawler DF (2003) Sphere drag and settling velocity revisited. *J Envir Engrg* 129:222–231.